Experimental comparison of three target acquisition models

Raviv Melamed, MEMBER SPIE
Yitzhak Yitzhaky, MEMBER SPIE
Norman S. Kopeika, MEMBER SPIE
Stanley R. Rotman, MEMBER SPIE
Ben-Gurion University of the Negev
Department of Electrical and Computer Engineering
P.O. Box 653
Beer-Sheva, IL-84105
Israel
E-mail: raviv@bguee.bgu.ac.il

Abstract. The role of the atmosphere in target acquisition modeling is investigated experimentally. Three models are compared to experimental results measured on the Golan Heights, Israel. Concepts considered are atmospheric attenuation versus atmospheric blur, and contrast-limited (blur-limited) versus noise-limited imaging. Results indicate that the role of the atmosphere in target acquisition is blur rather than attenuation and that for ranges of the order of a few kilometers, modern sensors are limited by atmospheric blur rather than by noise. A significant portion of the atmospheric blur derives from small angle forward scattering by aerosols, which actually increases measured temperature differences for ranges up to a few kilometers. [S0091-3286(98)00907-6]

Subject terms: thermal imaging; target acquisition; contrast; aerosols; modulation transfer function; turbulence; atmospheric optics; light scatter; blur.

Paper TAM-09 received Nov. 15, 1997; revised manuscript received Feb. 13, 1998; accepted for publication Feb. 13, 1998.

1 Introduction

Target acquisition models have been developed to quantify the quality of the image of a distant object seen by an observer who uses optical instrumentation. Images of distant objects are usually distorted by the atmosphere and optical instrumentation. These distortions affect the ability of an observer to extract information from the image about the given object. An accurate estimation of the probability of detection, recognition or identification will be reached only if a ''true to reality'' target acquisition model is used. Such models must include real life atmospheric effects, such as blur.

This paper compares three target acquisition models tested in an experiment held on the Golan Heights, Israel, in October 1996. The target acquisition models compared are:

Model a. standard Institute for Defense Analyses/U.S. Army Night Vision Laboratory (IDA/NVL) noise-limited target acquisition model,[1,2] which includes atmospheric transmission but not blur

Model b. IDA/NVL noise-limited target acquisition model corrected to include atmospheric blur[2,3]

Model c. contrast-limited target acquisition model,[2,4] which is also blur-limited.

All three models are summarized in Sections 11.2, 19.3 and 19.2, respectively, in Reference 2. These models are referred to here as models a, b and c, respectively.

2 Background

The spectrum of a target is multiplied by several modulation transfer functions (MTFs). The clarity of the image is therefore decreased. When the amplitude of the signal coming from the target is lower than the sensitivity threshold of the imaging system, it will not be detected by the imaging system and the energy that the signal was carrying will be lost. The loss of energy means a loss of information about the target. Since most of the energy lost is at high spatial frequencies, the image seen by the observer is blurred.

Imaging systems have several different detectors. Each detector has a sensitivity threshold. The overall sensitivity threshold of the imaging system derives from the highest among all the thresholds existing in the system. Common imaging systems have two sensitivity thresholds, the sensitivity threshold of the human eye (which is considered as a detector) and the sensitivity threshold of the electro-optical detectors.

The sensitivity threshold of the human eye depends directly on contrast. An imaging system whose MTF is limited by the contrast threshold is shown[2,4] in Fig. 1 and is called a contrast-limited system. The upper curve depicts the overall imaging-system MTF. The lower curve depicts the threshold contrast required by the observer. The spatial frequency at which both curves meet defines the maximum usable spatial frequency of the imaging system, designated here as $f_{r\,\max}$. Contrast-limited imaging thus involves a contrast limitation deriving from the overall system MTF and the threshold contrast of the observer at the output,[2,4] and blur deriving from the spatial frequency bandwidth limitation $f_{r\,\max}$.

On the other hand, the sensitivity threshold of electro-optical detectors depends directly on the noise level of the imaging system. When the sensitivity threshold of the electro-optical detectors is high, the imaging system is con-

 0091-3286/98/$10.00

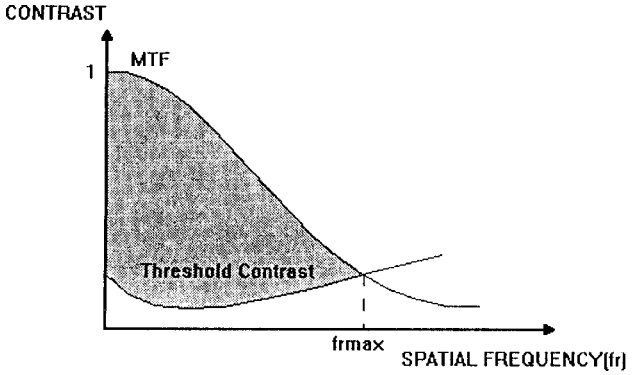

Fig. 1 Spatial frequency bandwidth ($f_{r\,\max}$) for contrast-limited imaging.

sidered to be ''noisy.'' A noisy image is characterized by random snow. Since the resolution of the imaging system is limited by a threshold caused by noise, it is called a noise-limited imaging system. The highest spatial frequency $f_{r\,\max}$ usable by an observer is derived from the point where both system and threshold signal-to-noise ratio (SNR) curves meet, as can be seen[2,4] in Fig. 2.

It is seen from Figs. 1 and 2 that whenever an image is contrast- or blur-limited $f_{r\,\max}$ in Fig. 1 will be smaller than $f_{r\,\max}$ in Fig. 2.

In terms of bar charts $f_{r\,\max}^{-1}$ represents the width of the narrowest equivalent line pair that can still be detectable by an observer, i.e.,

$$2\Delta x' \cong f_{r\,\max}^{-1}, \tag{1}$$

where $f_{r\,\max}$ represents the maximal spatial frequency that can still be detectable in the image and $\Delta x'$ represent the width of each line of this narrowest line pair in the image.[3] Since detail of size less than $(2\,f_{r\,\max})^{-1}$ is blurred, contrast-limited imagery is also blur-limited.

For different detection levels such as recognition and identification, several line pairs of width $f_{r\,\max}^{-1}$ placed over the critical dimension of the target x' are required,

$$x' = 2n\Delta x' \cong n f_{r\,\max}^{-1}, \tag{2}$$

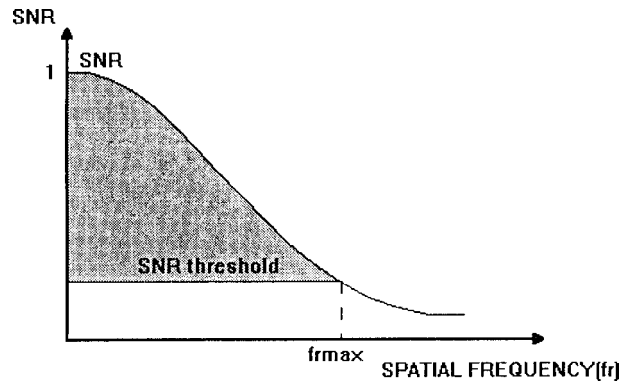

Fig. 2 Spatial frequency bandwidth ($f_{r\,\max}$) for noise-limited imaging.

where n is determined by the particular resolution criteria, the percentage of observers that can satisfy the specific resolution task, and the background clutter. The number n is derived from the Johnson[5,6] chart, which was developed in the late 1950s. Johnson was using image intensifier pictures with high SNRs for his experiments so that noise was not an issue. Thus, Johnson's imaging system was limited by contrast and the Johnson charts were developed originally for contrast-limited systems.[2,5,6]

Rosell[7] and Rosell & Wilson[8] expanded Johnson's work for low level light conditions and thus for noise-limited imaging systems. As thermal imaging systems developed research groups at the NVL tried to characterize observer performance with these imaging systems. The thermal imaging systems used by the NVL groups in those years were relatively ''noisy,'' therefore the models developed were for noise-limited imaging systems. The spatial frequency performance of noisy thermal imaging devices is characterized by the minimum resolvable temperature (MRT), which represents the noise threshold level as a function of spatial frequency in noise-limited systems such as shown in Fig. 2.

The effect of the atmosphere on a thermal signal in noise-limited models was represented in these IDA/NVL models by the atmospheric transmission factor τ, which is equal to

$$\tau = \exp\,(-\beta_{\text{atm}} R), \tag{3}$$

where β_{atm} is the path integrated average atmospheric extinction coefficient over path length R. As can be seen from Eq. (3), the atmosphere's role in noise limited models is to decrease the temperature difference of the signal coming from the target.

Evaluating the performance of a thermal imaging system was done by measuring its MRT. Since the MRT represents noise threshold level, an imaging system with lower MRT was considered to be a better one.

2.1 *Noise-Limited Model Based on Atmospheric Transmission (Model a)*

One of the widely used target acquisition models is the IDA/NVL target acquisition model (referred to here as model a). According to this model for every target acquisition mission, one can calculate the ratio of the atmospherically degraded thermal signal to the aspect corrected value of MRT. This ratio is called normalized SNR, given by[1,2]

$$\text{SNR} = K_\rho = \frac{\Delta T\,\exp\,(-\beta_{\text{atm}} R)}{\text{MRT}_0\,\exp\,(\gamma \beta_{\text{sys}} R/s)/(\epsilon/7)^{1/2}}, \tag{4}$$

where ΔT is the actual brightness temperature difference between the target and its background, ϵ is the aspect ratio of the target, and γ is the task difficulty function according to the Johnson criteria. For example, $\gamma = 1$ for detection and $\gamma = 4$ for recognition. Here MRT_0 is the MRT that can be detected when the target's spatial angular frequency approaches zero, and β_{sys} is the resolution coefficient of the imaging system. The system's MRT involves an approximation of the MRT curve to an exponential function and is given by[1,2]

$$\mathrm{MRT}=\mathrm{MRT}_0 \exp\,(\gamma\beta_{\mathrm{sys}}R/s)/(\epsilon/7)^{1/2}. \tag{5}$$

SNR can be calculated when the probability ρ of carrying out a given task of recognition or detection is given by

$$\rho=\frac{K_\rho^E}{1+K_\rho^E}, \tag{6}$$

where

$$E=2.7+0.7K_\rho. \tag{7}$$

The maximal distance R, in which the acquisition task is accomplished with the probability ρ, can be determined from Eq. (4) after determining K_ρ from Eq. (6).

As can be seen from Eq. (4), the IDA/NVL noise-limited target acquisition model characterizes the distortions of the target's signal caused by passing through the atmosphere and is characterized by a transmission function constant for all spatial frequencies according to Eq. (3).

2.2 *Noise-Limited Model Based on Atmospheric MTF (Model b)*

Since modern thermal imagers have significantly improved resolution over those in the 60s and 70s, distortions caused by the atmosphere to a thermal image significantly depend now on spatial frequencies.[2,3] Such atmospheric blur depends on two main factors, MTF due to turbulence and MTF due to scattering and absorption by aerosols. Watkins and Dutro[9] found that image degradation contains extinction losses from propagation as well as blurring due to atmospheric MTF, which is spatial frequency dependent. This limitation on contrast imposed by the atmosphere is blur rather than transmission. Transmission is included in atmospheric aerosol MTF, which describes blur caused in light scatter by aerosols.

2.2.1 *Turbulence MTF*

Turbulence results from random fluctuations in the atmospheric refractive index, which causes the light to arrive at different angles at the receiver. This results in image dancing, distortion, and blurring. The turbulence MTF for long exposures is represented by

$$\mathrm{MTF}_{\mathrm{le}}=\exp\,(-57.4a\nu^{5/3}C_n^2\lambda^{-1/3}R), \tag{8}$$

where a is unity for a plane wave and 3/8 for a spherical wave, λ is the measured radiation wavelength, C_n^2 is the turbulence strength factor, and ν is angular spatial frequency.

For short exposures (about 1 ms or less) the turbulence MTF is

$$\mathrm{MTF}_{\mathrm{se}}=\exp\,\{-57.4a\nu^{5/3}C_n^2\lambda^{-1/3}R[1-\mu(\nu/D)^{1/3}]\}, \tag{9}$$

where D is the aperture diameter of the imaging system and μ equals 0.5 in the far field and 1 in the near field.

Turbulence MTF can noticeably affect the higher spatial frequencies of thermal images.[2,3,9]

2.2.2 *Aerosol MTF*

In addition to turbulence, there are scattering and absorption caused by aerosols and molecules that exist in the atmosphere. Very little of the scattered light that is dispersed by aerosols reaches the imaging system mostly because of its limited field of view (FOV). Furthermore, some of the scattered light that reaches the receiver may not be detected because of the limited dynamic range of the detector and its limited bandwidth. Part of the unscattered light can be absorbed by such particulates. The scattering and absorption of energy by the aerosols affects all spatial frequencies, therefore causing edges in the image to be blurred and the image to be smoothed.

The aerosol MTF (approximated by a Gaussian form for simplification) is represented by[2–4,10–12]

$$\mathrm{MTF}(\nu)=\begin{cases}\exp\left[-A_aR-S_aR\left(\dfrac{\nu}{\nu_c}\right)^2\right], & \nu\leqslant\nu_c\\ \exp\,[-(A_a+S_a)R], & \nu\geqslant\nu_c\end{cases}, \tag{10}$$

where A_a and S_a are the atmospheric effective absorption and scattering coefficients, respectively, and ν_c is the angular spatial cutoff frequency at the aerosol MTF high frequency asymptote. In clear weather, ν_c is determined primarily by the optical instrumentation characteristics such as FOV, dynamic range and spatial frequency bandwidth of the imaging system.[4,10–12] In inclement weather, it is determined primarily by the aerosol size distribution.[2]

For $\nu\geqslant\nu_c$, aerosol MTF is approximately atmospheric transmission. However, at lower spatial frequencies measured atmospheric transmission is increased by small angle forward scatter as a function of spatial frequency. Therefore, ΔT in Eq. (4) is multiplied by Eq. (10) instead of by Eq. (3) to yield received temperature difference, which is[2,3]

$$\Delta T_r=\begin{cases}\Delta T_0\,\exp\left(-\dfrac{\beta_{\mathrm{atm}}}{R_c^2}R^3\right), & R\leqslant R_c\\ \Delta T_0\,\exp\,(-\beta_{\mathrm{atm}}R), & R\geqslant R_c\end{cases}, \tag{11}$$

where R_c is the cutoff range corresponding to the spatial angular cutoff frequency ν_c

$$R_c=\frac{\nu_c x}{\gamma}. \tag{12}$$

Consequently, a model was developed based on the IDA/NVL model but including the dependence of atmospheric blur on spatial frequency imposed on the image by the atmosphere. In other words, the noise-limited target acquisition model that was suggested is based on atmospheric MTF instead of atmospheric transmission. The atmospheric transmittance is included in the aerosol MTF and becomes an asymptote for high spatial frequencies if turbulence is weak. For ranges greater than R_c the asymptote of the aerosol MTF equals approximately the atmospheric transmit-

tance. The IDA/NVL model assumed that this equality exists for all distances, including those smaller than R_c. This assumption was contradicted in this experiment. Since for $\nu > \nu_c$ aerosol MTF approximately equals the atmospheric transmittance, in cases of weak turbulence model b agrees with the IDA/NVL model for $R > R_c$. For shorter ranges even in weak turbulence, these models are in disagreement.

The Ben-Gurion University model for noise limited model imaging (model b) is characterized for short exposures by[2,4]

$$\mathrm{SNR}=\begin{cases}\dfrac{\Delta T_0 \exp\left[-(\beta_{\mathrm{atm}}/R_c^2)R^3\right] \exp\left\{-57.4(\gamma/x)^{5/3}C_n^2\lambda^{-1/3}R^{8/3}[1-\mu(\gamma\lambda/sD)^{1/3}]\right\}}{\mathrm{MRT}_0 \exp\left[(\gamma/x)\beta_{\mathrm{sys}}R\right]/(\epsilon/7)^{1/2}}, & R \leqslant R_c \\ \dfrac{\Delta T_0 \exp\left(-\beta_{\mathrm{atm}}R\right) \exp\left\{-57.4(\gamma/x)^{5/3}C_n^2\lambda^{-1/3}R^{8/3}[1-\mu(\gamma\lambda/sD)^{1/3}]\right\}}{\mathrm{MRT}_0 \exp\left[(\gamma/x)\beta_{\mathrm{sys}}R\right]/(\epsilon/7)^{1/2}}, & R \geqslant R_c,\end{cases} \tag{13}$$

and for long exposures by

$$\mathrm{SNR}=\begin{cases}\dfrac{\Delta T_0 \exp\left[-(\beta_{\mathrm{atm}}/R_c^2)R^3\right] \exp\left[-57.4(\gamma/x)^{5/3}C_n^2\lambda^{-1/3}R^{8/3}\right)}{\mathrm{MRT}_0 \exp\left[(\gamma/x)\beta_{\mathrm{sys}}R\right]/(\epsilon/7)^{1/2}}, & R \leqslant R_c \\ \dfrac{\Delta T_0 \exp\left(-\beta_{\mathrm{atm}}R\right) \exp\left[-57.4(\gamma/x)^{5/3}C_n^2\lambda^{-1/3}R^{8/3}\right]}{\mathrm{MRT}_0 \exp\left[(\gamma/x)\beta_{\mathrm{sys}}R\right]/(\epsilon/7)^{1/2}}, & R \geqslant R_c\end{cases} \tag{14}$$

As seen in Eqs. (13) and (14), turbulence and aerosol MTFs are included in the numerators.

2.3 *Contrast-Limited Model Based on Atmospheric MTF (Model c)*

This third model[2,4] was also developed at the Ben-Gurion University for cases in which the imaging system is contrast- or blur-limited. Models for contrast-limited imaging systems are based mainly on Johnson's criteria, which was actually developed for contrast-limited imaging. The probabilities for target acquisition and acquisition time depend on the spatial frequency bandwidth of the imaging system. This bandwidth is derived from the point where both atmospheric MTF curve and human eye threshold contrast curves intersect, as shown in Fig. 1.

Schulze[13] approximated the human eye threshold contrast curve as

$$\otimes\mathrm{eye}\,(\nu)=\frac{\nu_e}{\exp\,(-c_1\nu)-\exp\,(-c_2\nu)}, \tag{15}$$

where $\otimes$eye is the threshold contrast required by the human visual system, ν in cycles per degree, $\nu_e=0.001033$, $c_1=0.1138$ deg and $c_2=0.325$ deg.

Fig. 3 describes this approximation of the human eye threshold contrast curve which is especially accurate at higher spatial frequencies. The spatial frequency at the cross point of the curves determines the minimal number of line pairs over the minimum image dimension of the target that can be resolved by the observer. This spatial frequency, which is designated in Fig. 1 as $f_{r\,\max}$, is the target's maximal resolvable frequency and therefore determines the probability of various acquisition tasks.[2,4]

For angular spatial frequency $\nu_{\max}$ corresponding to spatial frequency $f_{r\,\max}$, the number of resolvable line pairs n over target critical dimension x for a given probability of acquisition task can be determined from[2,4]

$$n=\nu_{\max}x/R. \tag{16}$$

The probability of acquisition equals

$$\rho=\frac{(n/n_{50})^E}{1+(n/n_{50})^E}, \tag{17}$$

where

$$E=2.7+0.7(n/n_{50}), \tag{18}$$

and n_{50} is the number of line pairs over the target critical dimension from the Johnson chart.[2,5,6]

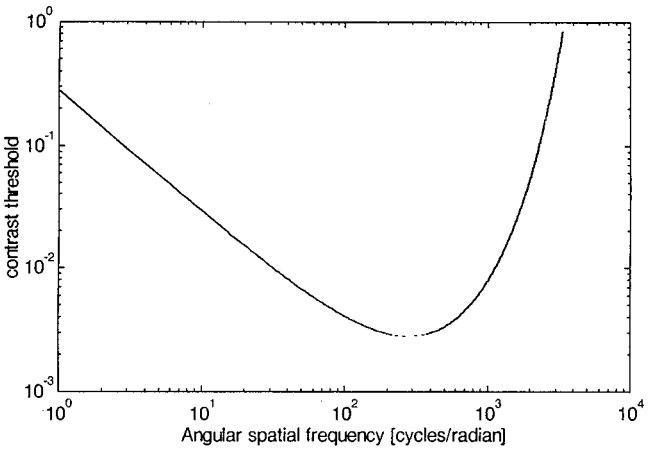

Fig. 3 Human vision threshold contrast approximated by Eq. (15).

Table 1 Meteorological data measured in the experiment.

Time	Wind Direction	Wind Velocity (m/s)	Air Temperature (C)	Effective Temperature (C)	Deep Temperature (C)	Surf Temperature (C)	Relative Humidity (%)	Pressure (mbar)
1545	258.8	6.653	25.01	28.55	25.01	28.55	39.09	937
1600	271.1	5.338	25.07	28.46	25.07	28.46	37.74	937
1615	271.3	5.531	24.57	27.96	24.57	27.96	37.93	937
1630	281	4.952	24.02	26.84	24.02	26.84	39.2	937
1645	287.6	4.098	23.62	25.82	23.62	25.82	41.57	937
1700	283.6	4.086	23.01	24.68	23.01	24.68	45.03	936
1715	301.7	2.754	22.52	23.35	22.52	23.35	44.1	936
1730	296.9	2.492	21.94	21.96	21.94	21.96	53.57	936
1745	294.8	2.252	21.62	21.25	21.62	21.25	54.73	936
0000	299.4	0.815	17.58	16.6	17.58	16.6	82.4	936
0015	299.8	1.202	17.94	16.74	17.94	16.74	82	935
0030	304.4	0.986	17.94	16.89	17.94	16.89	81.7	935
0045	312.2	0.948	17.8	16.81	17.8	16.81	82.3	935

Today, most thermal imaging systems have very low noise levels because of the technology used in thermal detectors. Therefore, most images are not noise-limited, i.e., snowy, but rather contrast- or blur-limited. As a result, target acquisition modeling will be improved by returning to Johnson's original modeling, which was for contrast-limited imaging and expanding it to include atmospheric MTF, which, for long ranges, limits the resolution more than the hardware does.[2,4,12] Although in most cases with modern imaging systems the image is contrast- or blur-limited, there are some cases where the image may be noise-limited. Therefore noise- and contrast-limited models should be considered as complementary models. Both models should include effects of the atmospheric MTF to describe blur rather than transmission.[2]

3 Experiment

A comparison of the three target acquisition models described here was performed to find the model closest to reality as reflected in our experiment. The experiment was held October 8, 1996, on the Golan Heights, Israel. For our experiment we used a 2.2×2.2 m bar chart, which was placed at distances of 60 m, 1 km, and 2.3 km. The pictures of the bar charts and a GMC truck, which was placed next to it were taken in the late afternoon and at midnight with Amber's Radiance 1 camera. The camera's focal length was 250 mm and its field of view was 38.9 mrad. Meteorological data for the day of the experiment are given in Table 1.

To determine the camera's MTF we took pictures of the bar charts placed at a distance of 60 m, measured the image edge response,[2,11] and derived the imaging system MTF. We did the same procedure for bar charts and targets at distances of 1 and 2.3 km and found atmospheric plus hardware MTFs for these distances, as shown in Figs. 4 and 5. To determine the atmospheric MTF, the atmospheric plus hardware MTFs were divided by the hardware MTF. As range increases atmospheric MTF becomes more dominant over hardware MTF. Figs. 6(a) and 6(b) show the actual and restored images (using an atmospheric Wiener filter[2,14])

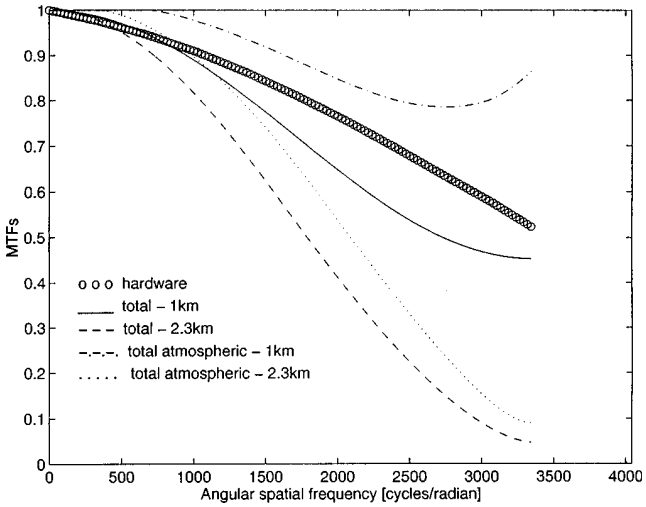

Fig. 4 Total, hardware and atmospheric MTFs for 1 and 2.3 km imaging distance.

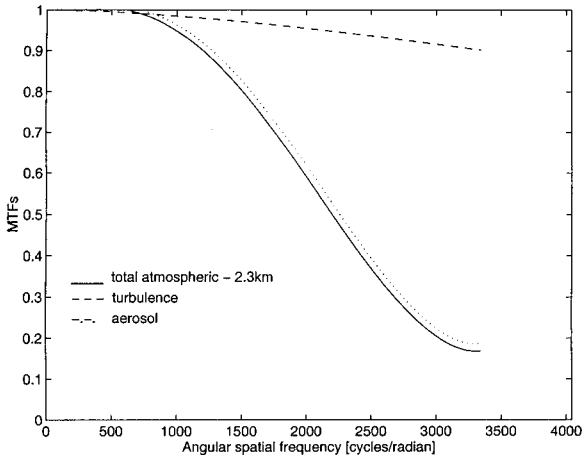

Fig. 5 Atmospheric MTF and its aerosol and turbulence MTF components (Ref. 23) for 2.3 km distance.

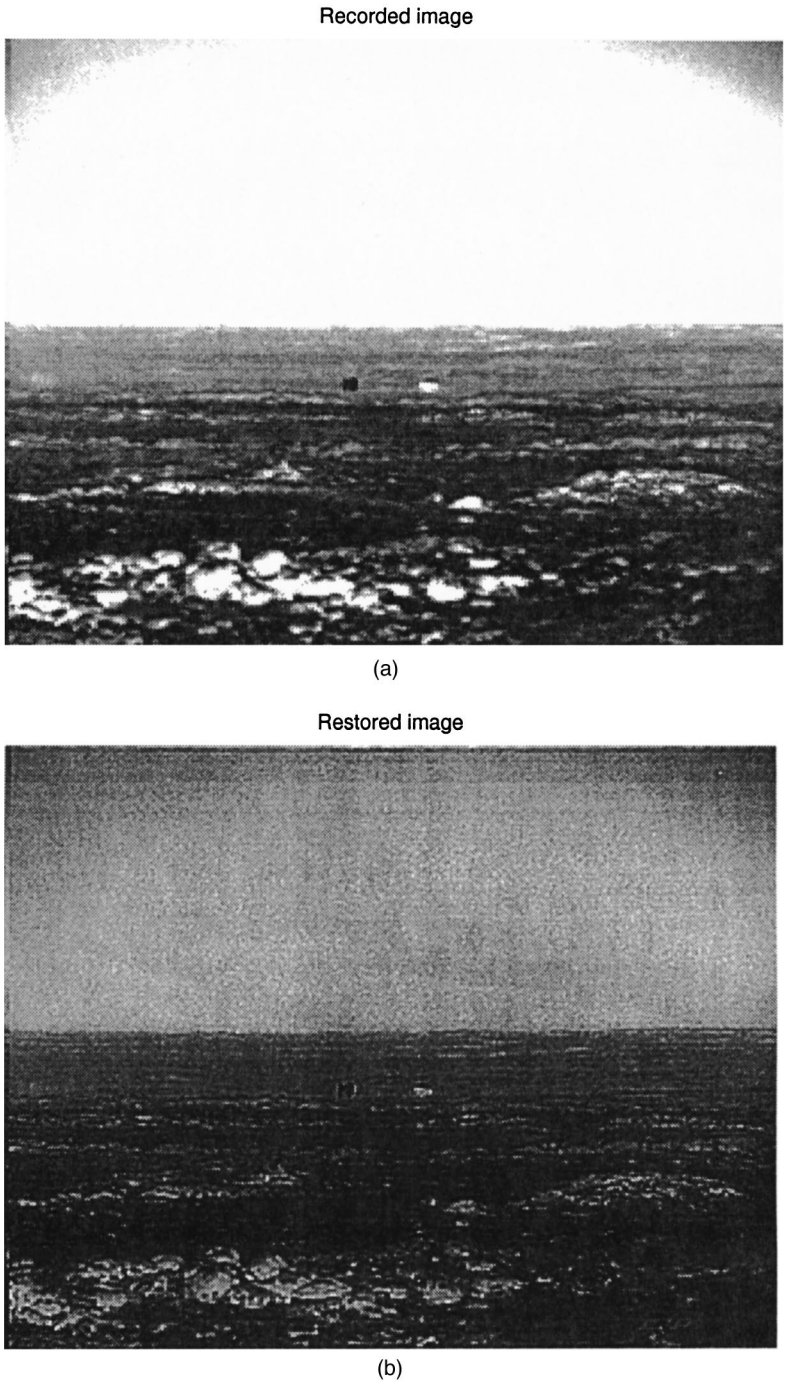

Fig. 6 (a) Recorded image (2.3 km distance) and (b) restored image using atmospheric MTF with an atmospheric Wiener filter.

for the 2.3 km range. The restored image indicates the vertical bars in the resolution chart are not uniform but affected by reflections from the sky. This may decrease the apparent ΔT. This is emphasized here because as shown later, the apparent or measured ΔT was actually greater than expected from atmospheric transmission.

4 Results

The three models were compared in two steps. First, the necessity to include atmospheric blur in the noise-limited models was confirmed by comparing models a and b. Then a comparison between models b and c was made.

4.1 *Atmospheric Transmission versus Atmospheric MTF*

As described, the difference between model a and model b is that in model b the signal that reaches the imaging system is multiplied by the atmospheric MTF and not by the atmospheric transmittance, as done in model a.

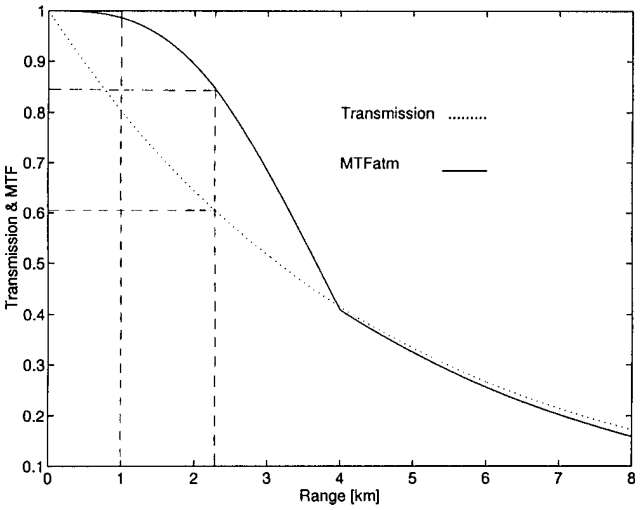

Fig. 7 Expected atmospheric transmission and atmospheric MTF versus range in the experiment that was held in the afternoon; the 1 and 2.3 km ranges are marked off.

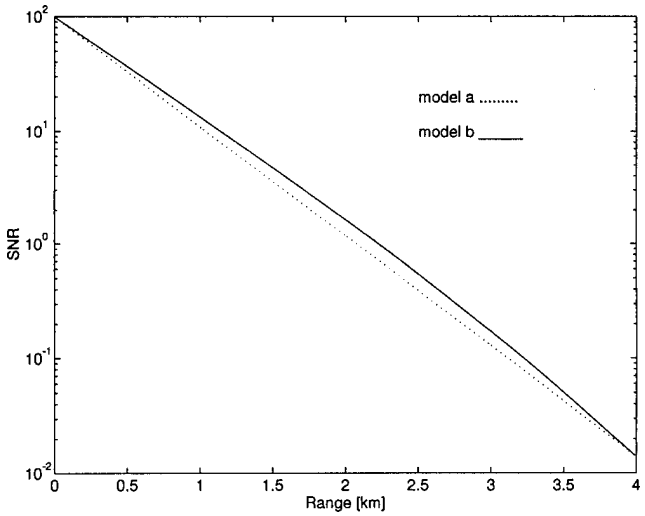

Fig. 9 Expected SNR versus range in the experiment that was held in the afternoon.

Figure 7 shows the range dependent atmospheric transmittance and atmospheric MTF used in models a and b measured in the late afternoon and calculated using Eqs. (3), (9) and (10). The expected degradation of the target ΔT at both distances according to these models is also noted. Fig. 8 shows the range dependent atmospheric transmittance and atmospheric MTF used in models a and b measured at midnight and calculated using Eqs. (3), (9) and (10). The expected degradation of the target ΔT at both distances according to these models is also noted.

Since turbulence was weak (Fig. 5) the atmospheric MTF curve coincides with the atmospheric transmittance curve for $R>R_c$ in Figs. 7 and 8. It is to be expected that for strong turbulence the atmospheric MTF curve will be lower for all ranges and will not coincide with the atmospheric transmittance curve for $R>R_c$.

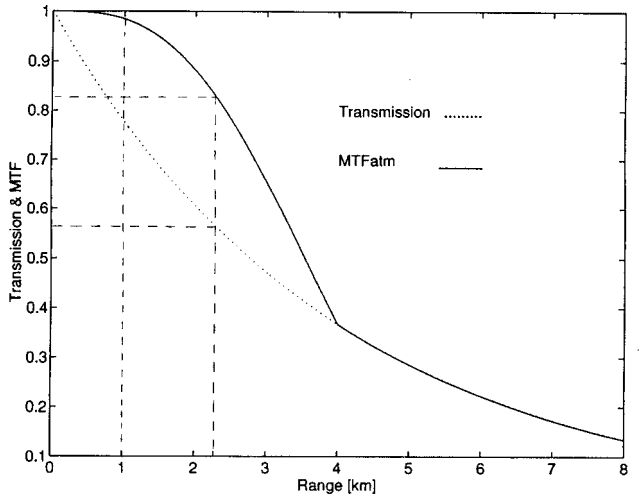

Fig. 8 Expected atmospheric transmission and MTF versus range in the experiment that was held at midnight; 1 and 2.3 km ranges are marked off.

Figs. 9 and 10 shows the SNR according to Eqs. (4) and (13). It can be seen from the figures that the transmission of the atmosphere at distances smaller than R_c predicted by model b is higher than that of model a.

The measurements of the atmospheric transmission at the relevant spatial frequencies were performed by measuring ΔT as the difference in gray levels between the black bar and the white bar of a thermal target placed 60 m from the imaging system. Measuring ΔT was done by averaging the gray levels at the middle of each bar and then subtracting the results. This measurement gives the signal strength emitted from the target.

The procedure was repeated again for images at distances of 1 and 2.3 km from the camera. In these measurements the pixels in the image that were averaged were the same pixels that were averaged for targets at a distance of 60 m. The temperature differences that were measured at distances of 1 and 2.3 km are presented in the column entitled measured transmission in Table 2. Table 2 summarizes the degradation of ΔT measured in the late afternoon at different distances. The results in the columns entitled expected transmission for model b and expected transmission for model a were calculated by multiplying the temperature difference of the close target (60 m) with the atmospheric transmittance or atmospheric MTF, depending on the model used, as described by

$$\Delta T_r = \Delta T_0 \exp(-\beta_{\text{atm}} R) \tag{19}$$

for model a, and

$$\Delta T_r = \Delta T_0 \exp\left(-\frac{\beta_{\text{atm}}}{R_c^2} R^3\right) \times \exp\left\{-57.4\left(\frac{\gamma}{s}\right)^{5/3} C_n^2 \lambda^{-1/3} R^{8/3}\left[1-\mu\left(\frac{\gamma\lambda}{sD}\right)^{1/3}\right]\right\} \tag{20}$$

for model b, which includes the atmospheric MTF.

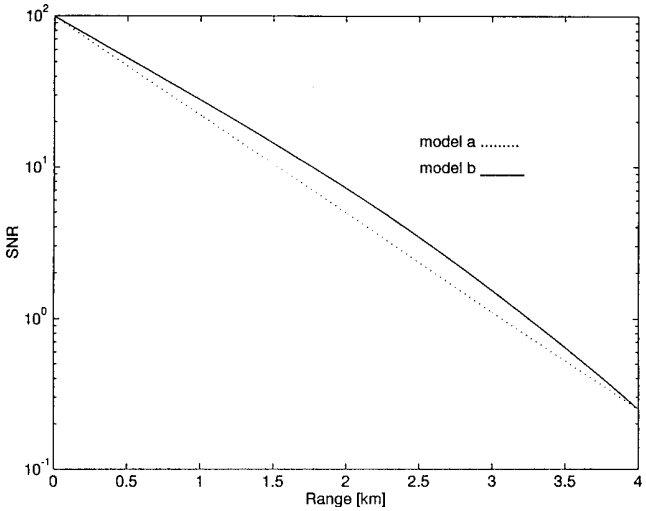

Fig. 10 Expected SNR versus range in the experiment that was held at midnight.

In Eqs. (19) and (20), R was taken as 1 and 2.3 km (from these distances we subtracted 60 m). The angular spatial frequencies that were used for the calculations in Eq. (20) were the frequencies of the bar chart (1 cycle/mrad for 1 km and 2.3 cycles/mrad for 2.3 km). It can be assumed that the high atmospheric transmission that was measured in the experiment and is shown in Table 2 results from measuring the transmission at these low angular spatial frequencies. Analysis of the aerosol MTF knee indicates atmosphere transmittance is of the order of 70% per 1 km distance, which yields $\beta_{\text{atm}} = 0.36\ \text{km}^{-1}$. Analysis with LOWTRAN 7 indicates that much of the attenuation (about 60%) is absorption. At low angular spatial frequencies the aerosol MTF had only a very small attenuation effect on the atmospheric transmission. Conservation of energy implies light that was scattered cannot also be absorbed by the same particulate. Therefore, particulate (including both molecules and aerosols) absorption affects mostly the high spatial frequency region of the aerosol MTF (which involves the unscattered light image), and the low spatial frequency region (which involves the scattered light image) is hardly subject to it.[15] This helps explain why the expected transmission and the measured transmission using model b are higher than expected for model a, since absorption decreases aerosol MTF primarily at high spatial frequencies and much less at low ones.[15] The high ΔT measured according to gray levels cannot be explained by atmospheric transmission but can be explained by aerosol MTF.

Table 2 Expected transmission of ΔT according to models a and b versus observed transmission at different distances.

Distance (km)	Expected Transmission Using Model a	Expected Transmission at Bar Target Frequency Using Model b	Measured Transmission
1	0.6977	0.9774	0.94
2.3	0.437	0.7577	0.85*

*See the Appendix.

It can be seen clearly from the results presented in Table 2 that model b depicts reality as reflected in the experiment much better than does model a. The reason is that small angle forward scatter causes the middle of the white bar image to be much whiter because radiation from nearby regions in the white bar object is also imaged into the middle of the white bar image. Such small angle forward scatter effects are not considered or included in model a. This forward scatter causes the measured transmission at low spatial frequencies to be higher than expected from Eq. (3). The significant role of the aerosol MTF is thus confirmed in Table 2, which clearly supports target acquisition model b.

4.2 *Noise-Limited Model versus Contrast-Limited Model*

Having seen that atmospheric effects on target acquisition are blur rather than transmission, we now compare models b and c, both of which include atmospheric blur in the form of atmospheric MTF. The comparison between models b and c is performed by finding probabilities of detection, recognition, and identification for both models and comparing them with the ability to detect or recognize targets in the images.

From a close look at the model equations it is to be expected that if the image is contrast- or blur-limited (when the eye contrast threshold is higher than the noise threshold), then model c will result in a lower probability to perform a target acquisition task than model b.

The noise threshold, which is represented by the MRT, was found by using the FLIR92 model with the data which was given by the Amber Radiance 1 manufacturer. The results were also compared with the manufacturer results.

The curves of the noise threshold (MRT); the eye contrast threshold, as calculated using Eq. (15); and the total measured system MTF (calculated from the system edge response) are shown in Fig. 11 for pictures that were taken in the late afternoon and in Figs. 12 and 13 for pictures that were taken at midnight. It should be noted that the imaging system's cutoff frequency (nyquist frequency) as limited by the hardware was only 3269 cy/radian.

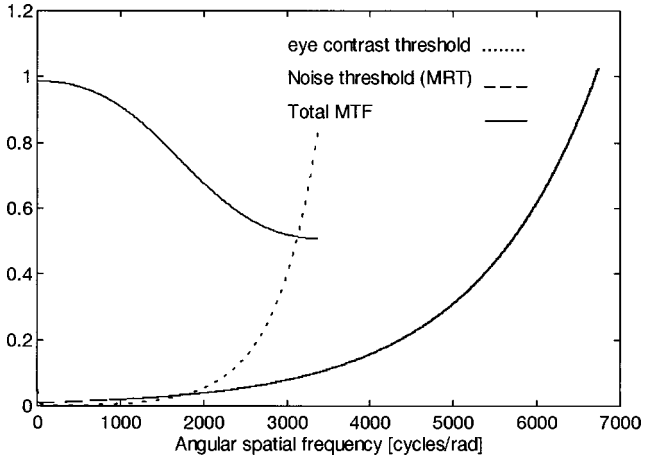

Fig. 11 Total MTF, noise threshold (MRT) and contrast threshold versus angular spatial frequency in the experiment held in the afternoon. Range is 1 km.

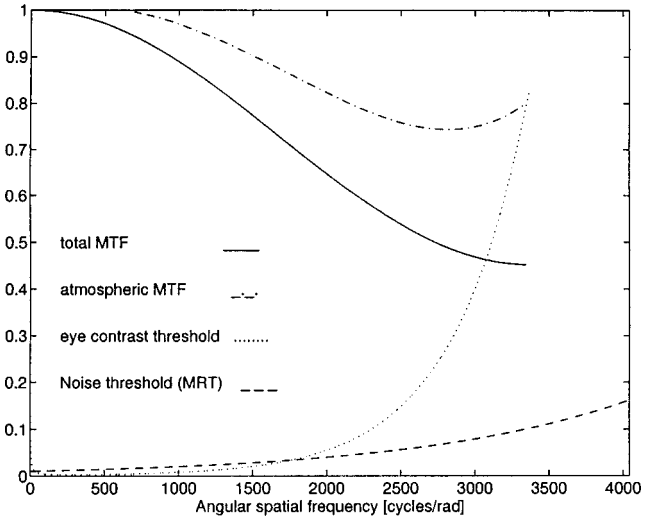

Fig. 12 Total MTF, atmospheric MTF, noise threshold (MRT) and contrast threshold versus angular spatial frequency in the experiment held at midnight. Range is 1 km.

The maximal resolvable angular spatial frequency in a noise-limited image is the frequency where the noise threshold curve (MRT) crosses the atmospheric MTF curve instead of the total system MTF curve because the MRT curve already includes the hardware MTF. On the other hand, the maximal resolvable angular spatial frequency in a contrast-limited image is the frequency where the eye contrast threshold curve intersects the total MTF curve, which includes the hardware MTF and the atmospheric MTF.

As illustrated in Figs. 11, 12 and 13, the angular spatial frequency bandwidth is limited by the higher threshold (the one that limits the maximal resolvable angular spatial frequency) and that is the eye contrast threshold. It can be seen that the noise level of a modern camera such as Radiance 1 is very low.

Because of the system's hardware limitation, the real cutoff frequency of the imaging system is limited by FOV

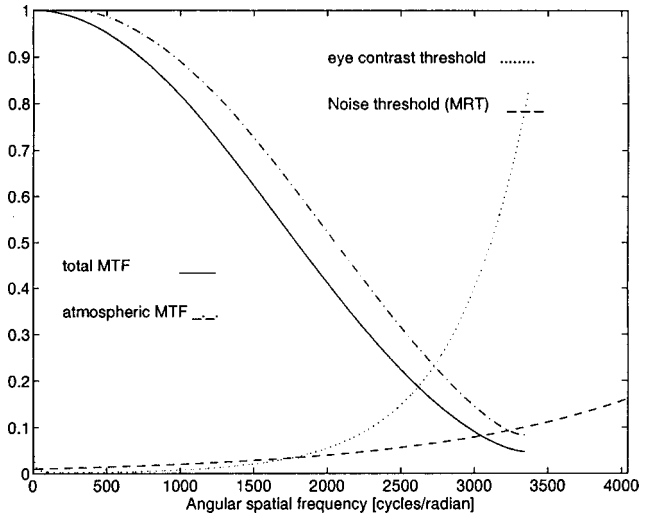

Fig. 13 Total MTF, atmospheric MTF, noise threshold (MRT) and contrast threshold versus angular spatial frequency in the experiment held at midnight. Range is 2.3 km.

Table 3 Maximal spatial angular frequency ($f_{r\,\max}$) in the experiments. Hardware cutoff frequency is 3269 cycles rad^{-1}.

Experiment	$f_{r\,\max}$ for Noise Threshold (cycles/rad)	$f_{r\,\max}$ for Contrast Threshold (cycles/rad)
Afternoon, 1 km	3269	3126
Midnight, 1 km	3269	3073
Midnight, 2 km	3233	2616

and equals 3269 cycles/rad. This limitation means that the noise threshold curve does not behave as shown in Figs. 11–13 but goes straight up at the hardware cutoff frequency. Table 3 shows the maximal resolvable angular spatial frequencies for both thresholds. For noise-limited imaging it is the hardware limit, since the noise is so low.

For presentation of probabilities of recognition and detection as a function of distance from the target, Eqs. (16) to (18) were used. Fig. 14 shows the probability of recognition as a function of range from the target for models b and c in the experiment that was held in the late afternoon. Figs. 15 and 16 show the probability of recognition as a function of range from the target for models b and c in the experiments that were held at midnight. The results seen in Figs. 14–16 were calculated for the recognition task ($n_{50}=4$). The results seen in Figs. 17–19 were calculated for the identification task ($n_{50}=6.4$).

Comparison between the results and the pictures that were taken shows that model c, which was developed for contrast- or blur-limited imaging systems, although being more pessimistic, depicts reality better than does model b.

The maximal resolvable angular spatial frequency in a noise-limited image is the frequency where the MRT curve and the atmospheric MTF curve meet. The maximal angular spatial frequency that was used for calculations was the cutoff frequency of the imaging system. Therefore, if the imaging system had a narrower FOV the maximal angular spatial frequency $f_{r\,\max}$ that was used for calculations would have been higher. A higher value of $f_{r\,\max}$ or a wider

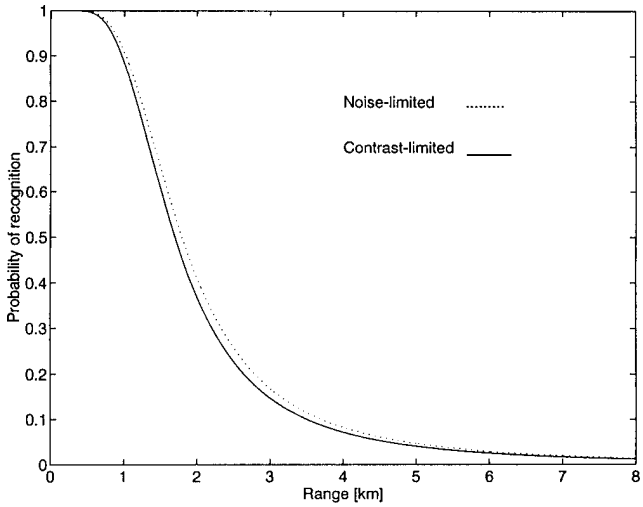

Fig. 14 Probability of recognition versus range for the afternoon experiment. Range is 1 km.

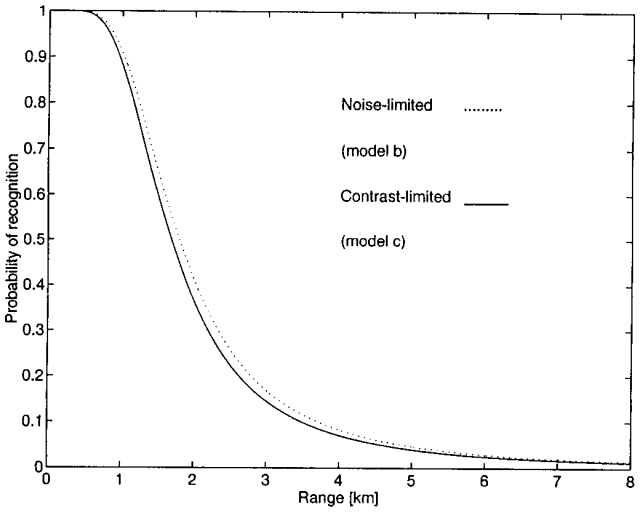

Fig. 15 Probability of recognition versus range for the midnight experiment. Range is 1 km.

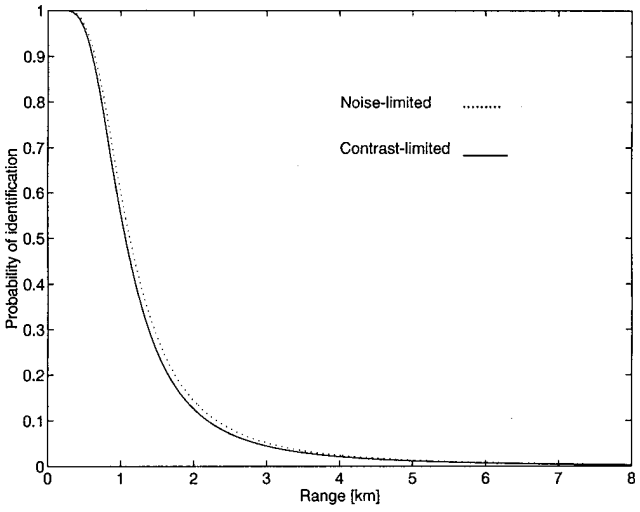

Fig. 17 Probability of identification versus range for the afternoon experiment. Range is 1 km.

spatial frequency bandwidth enables higher probability to accomplish an acquisition task. Thus, using a higher maximal angular spatial frequency would cause the curves in Figs. 17–19, which represent the probability of a target acquisition task for noise-limited models, to move to the right and enable identification at distances close to 2 km.

Figure 20 shows the probability of identification when using the theoretical maximal angular spatial frequency limited by the atmospheric blur (derived from the cross point of the MRT curve and the atmospheric MTF curve) and not the cutoff frequency of the imaging hardware. Fig. 21 shows the GMC truck at a distance of 1 km. It is at around pixel coordinates (150,140). It can be seen easily that an identification task cannot be accomplished, nor can recognition. Model c, which is more pessimistic, is therefore a closer match to experiment than model b.

Although in Table 2 there is very good correlation between measured transmission and transmission expected from model b using atmospheric MTF instead of transmission, the correlation at 2.3 km is poorer. Fig. 21 suggests the reason for the poorer correlation at 2.3 km is that models a and b are noise-limited while in reality the image is contrast- or blur-limited.

5 Conclusions

The results of the experiment show that using one extinction coefficient at all angular spatial frequencies for target acquisition is inappropriate. The atmosphere has a different effect at each spatial frequency. This indicates target acquisition is limited by atmospheric blur rather than transmission.

When the distance to the target is less than R_c, averaging several pixels of the white bar shows there is an addition of white light that was forward scattered at small angles. Therefore, there is an increase in the amount of white light compared to the noise-limited models such as the IDA/NVL model (model a) that do not include forward

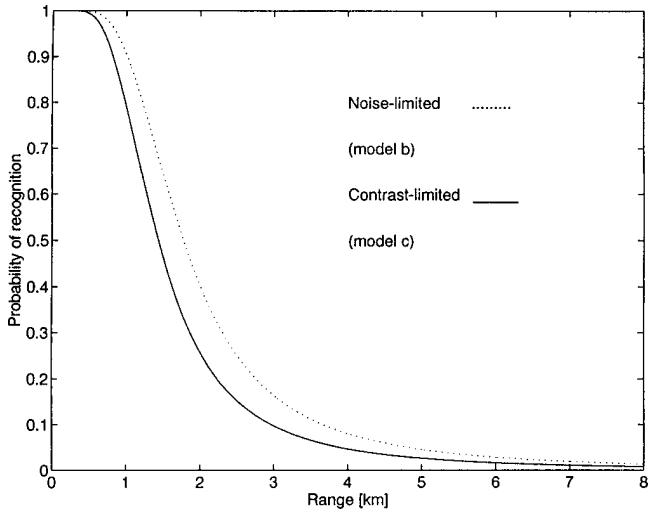

Fig. 16 Probability of recognition versus range for the midnight experiment. Range is 2.3 km.

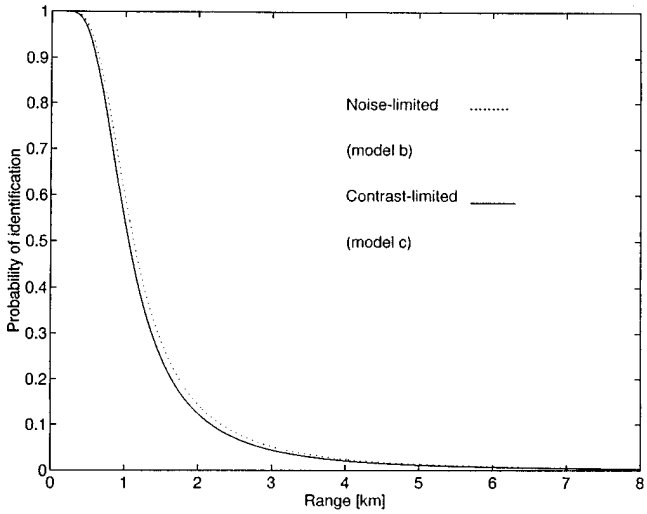

Fig. 18 Probability of identification versus range for the midnight experiment. Range is 1 km.

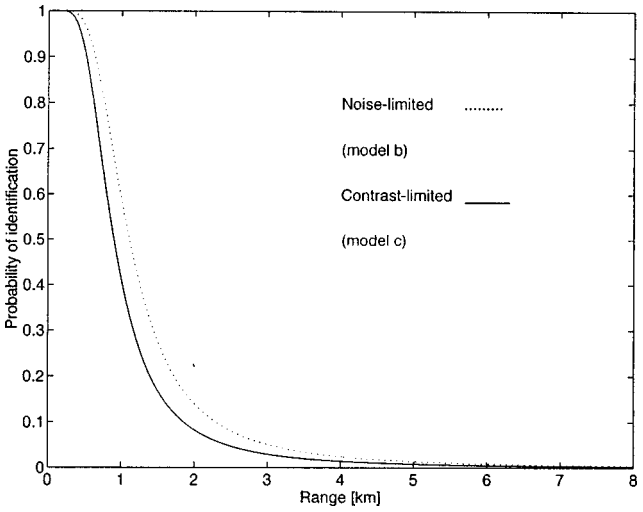

Fig. 19 Probability of identification versus range for the midnight experiment. Range is 2.3 km.

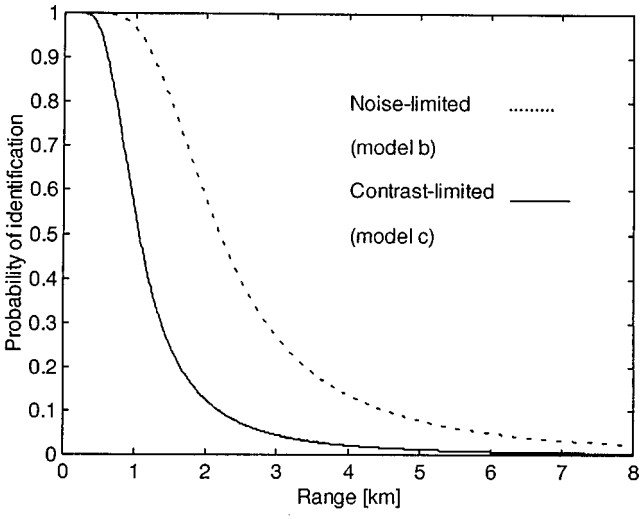

Fig. 20 Estimated probability of identification versus range for the midnight experiment assuming MRT intersects MTFatm. Range is 2.3 km.

scattering at small angles. This means that the measured difference in temperatures ΔT is larger than the temperature difference calculated from model a. Thus, atmospheric blur effects should be included in the NVL/IDA model, which was developed for noise-limited imaging systems (model a). This experiment supports model b.

Furthermore, the comparison made between model b (noise-limited) and model c (contrast-limited), both of which include atmospheric blur rather than transmittance, shows that the imaging system was contrast- or blur-limited and therefore the maximal angular spatial frequency that is used to calculate the probability to accomplish an acquisition task is derived from the point where both atmospheric MTF curve and the human eye threshold contrast curve intersect. This probability was lower than the one obtained when model b was used and thus supports model c. This result is supported by the pictures that were taken in the experiment, which are consistent only with the more pessimistic of models b and c. Comparison of models b and c indicates the limitations to target acquisition were imposed by atmospheric blur rather than by noise.

In these experiments, the dominant source of atmospheric blur is seen to derive from forward scattering by aerosols, which also explains the much larger temperature difference ΔT actually measured than was expected from atmospheric transmission. The strong blur effect caused by aerosols has been well known for many years in satellite imagery, where it is called the adjacency effect,[16–21] since forward small angle scatter by aerosols cause photons to be imaged in pixels *adjacent* to where they should be, even in

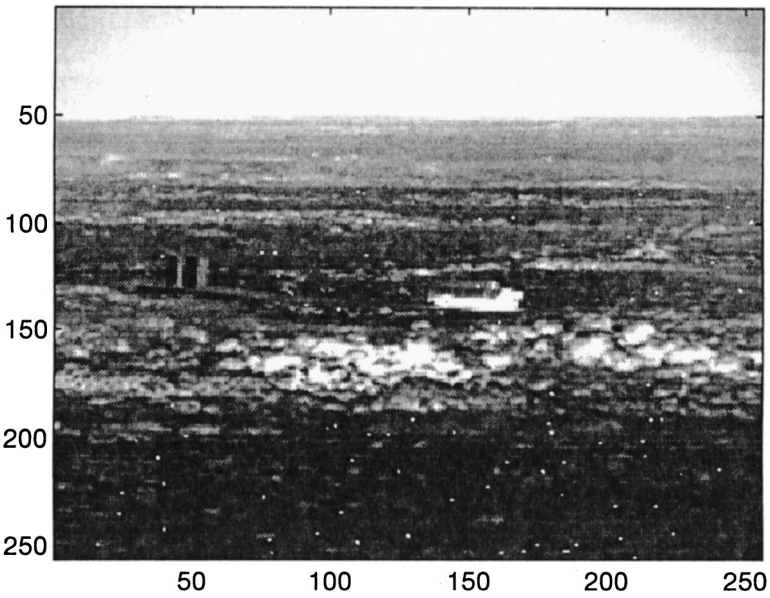

Fig. 21 Recorded image of the GMC truck. Range is 1 km.

the visible where turbulence has more effect than in the IR. It therefore should not be surprising to see here how significant aerosol MTF is in the IR, as noted previously.[12,22] These experiments suggest that model c is the most realistic one for target acquisition in view of the low noise characteristics of modern sensors.

6 Appendix

When the distance was changed from 1 to 2.3 km, the camera's nonuniformity correction (NUC) was changed from NUC 1 to NUC 4, respectively. Changing the camera's NUC results in a change of its integration time. The integration time using NUC 1 is 0.313 ms and using NUC 4 is one half of this, or 0.157 ms.

A pixel's gray level is

$$\text{Gray level} = A + BK\text{IT} \exp(-\beta_{\text{atm}} R), \tag{A1}$$

where A is the dc offset, B is the calibration constant of the camera, K is radiance of the target (which is assumed to be constant) and IT is the integration time of the camera. Subtracting two gray levels (ΔT) will cancel the dc offset A. A division of $2\Delta T$ will cancel the multiplication factors B, K and IT and omit the atmospheric transmittance. In our case, the result of this division (when the change of NUC was not taken into account) was 0.427. This result was multiplied by 2 since the IT was doubled when the camera's NUC was changed from NUC 1 to NUC 4. Therefore, the atmospheric transmittance that was measured in the experiment was 0.854.

Acknowledgments

The authors are grateful to Dr. Motti Zeller for his support and assistance regarding the Amber thermal imager.

References

1. L. N. Seekamp, ''Field manual to determine detection or recognition range of a flir sensor,'' Institute for Defense Analyses, IDA paper p-1419 (Sep. 1979).
2. N. S. Kopeika, *A System Engineering Approach to Imaging*, SPIE Optical Engineering Press, Bellingham, WA (1998).
3. D. Sadot, N. S. Kopeika, and S. R. Rotman, ''Incorporation of atmospheric blurring effects in target acquisition modeling of thermal images,'' *Infrared Phys. Technol.* **36**, 551–564 (1995).
4. D. Sadot, N. S. Kopeika, and S. R. Rotman, ''Target acquisition modeling for contrast-limited imaging: effects of atmospheric blur and image restoration,'' *J. Opt. Soc. Am. A* **12**, 2401–2414 (1995).
5. J. Johnson, ''Analysis of image forming systems,'' in *Proc. Image Intensifier Symp.*, pp. 244–273, AD 220160 Warfare Electrical Engineering Department, U.S. Army Research and Development Laboratories, Ft. Belvoir, VA (1958).
6. J. Johnson, ''Analytical description of night vision devices,'' in *Proc. of Seminar on Direct-Viewing Electro-Optical Aids to Night Vision*, L. M. Biberman, Ed., pp. 177–200, Institute for Defense Analyses Study 52254 Institute for Defense Analyses, Alexandria, VA (1966).
7. F. A. Rosell, ''Television camera tube performance data and calculations,'' in *Photoelectronic Imaging Devices: Vol. 2, Devices and Their Evaluation*, L. M. Biberman and S. Nudelman, Eds., pp. 527–577, Plenum, New York (1971).
8. F. A. Rosell and R. H. Wilson, ''Recent psychophysical experiments and the display signal to noise ratio concept,'' in *Preception of Displayed Information*, L. M. Biberman, Ed., pp. 167–232, Plenum, New York (1973).
9. W. Watkins and R. Dutro, ''Contrast transmission predictions versus far-infrared imager measurements for low-altitude horizontal paths,'' *Opt. Eng.* **33**, 2588–2593 (1994).
10. D. Sadot and N. S. Kopeika, ''Imaging through the atmosphere: practical instrumentation-based theory and verification of aerosol modulation transfer function,'' *J. Opt. Soc. Am. A* **10**, 172–179 (1993).
11. I. Dror, N. S. Kopeika, ''Experimental comparison of turbulence MTF and aerosol MTF through the open atmosphere,'' *J. Opt. Soc. Am. A* **12**, 970–980 (1995).
12. D. Sadot, G. Kitron, N. Kitron, and N. S. Kopeika, ''Thermal imaging through the atmosphere: atmospheric MTF theory and verification,'' *Opt. Eng.* **33**, 880–887 (1994).
13. T. J. Schulze, ''A procedure for calculating the resolution of electro-optical systems,'' in *Airborne Reconnaissance XIV*, F. R. LaGesse, P. A. Henkel, and W. W. Schurter, Eds., *Proc. SPIE* **1342**, 317–327 (1990).
14. D. Sadot, A. Rosenfeld, G. Shuker, and N. S. Kopeika, ''High-resolution restoration of images distorted by the atmosphere, based on an average atmospheric MTF,'' *Opt. Eng.* **34**, 1799–1807 (1995).
15. D. Sadot and N. S. Kopeika, ''Effects of absorption on image quality through a particulate medium,'' *Appl. Opt.* **30**, 7107–7111 (1994).
16. J. Otterman and R. Fraser, ''Adjacency effects on imaging by surface reflection and atmospheric scattering: cross radiance to zenith,'' *Appl. Opt.* **18**, 2852–2860 (1979).
17. Y. Kaufman, ''Atmospheric effect on spatial resolution of surface imagery,'' *Appl. Opt.* **23**, 4164–4172 (1984).
18. W. Pearce, ''Monte Carlo study of the atmospheric spread function,'' *Appl. Opt.* **25**, 438–447 (1986).
19. D. Tanre, C. Devaux, M. Herman, and R. Samter, ''Radiative properties of desert aerosols by optical ground-based measurements at solar wavelengths,'' *J. Geophys. Res.* **93**, 14223–14231 (1988).
20. P. N. Reinersman and K. L. Carder, ''Monte Carlo simulation of the atmospheric point spread function with an application to correction for the adjacency effect,'' *Appl. Opt.* **34**, 4453–4471 (1995).
21. E. F. Vermote, N. El Saleous, C. O. Justice, Y. J. Kaufman, J. L. Privette, L. Rener, J. C. Roger, and D. Tanre, ''Atmospheric correction of visible to middle-infrared EOS-MODIS data over land surfaces: background, operational algorithm, and validation,'' *J. Geophys. Res.* **102**, 17131–17141 (1997).
22. D. Sadot, A. Dvir, I. Bergel, and N. S. Kopeika, ''Restoration of thermal images distorted by the atmosphere, based upon measured and theoretical atmospheric MTF,'' *Opt. Eng.* **33**, 44–53 (1994).
23. D. Sadot, S. Shamriz, I. Sasson, and N. S. Kopeika, ''Prediction of overall atmospheric MTF with standard weather parameters: comparison with measurements with two imaging systems,'' *Opt. Eng.* **34**, 3239–3248 (1995).

Raviv Melamed received his BSc degree in 1994 in electrical engineering from Ben-Gurion University of the Negev. He is now an MS student in the Department of Electrical and Computer Engineering at Ben-Gurion University of the Negev. His current research interest is target acquisition modeling. He is a member of SPIE.

Yitzhak Yitzhaky received his BSc and MSc degrees in electrical and computer engineering from Ben-Gurion University of the Negev, Israel, in 1993 and 1995, respectively. Presently he is a PhD research assistant and student in the electro-optics and image processing program at the same university. His current research interests are in restoration of images blurred by motion or atmosphere. He is a member of SPIE.

Norman S. Kopeika: Biography appears with the paper ''Relative effects of distortion and noise on target acquisition: the advisability of image restoration'' in this issue.

Stanley R. Rotman: Biography appears with the paper ''Relative effects of distortion and noise on target acquisition: the advisability of image restoration'' in this issue.